

# Optimal protocol for collisional Brownian engines

Gustavo A. L. Forão<sup>1</sup>

<sup>1</sup>*Universidade de São Paulo, Instituto de Física, Rua do Matão, 1371, 05508-090 São Paulo, SP, Brazil*

(Dated: June 6, 2025)

Collisional Brownian engines have recently gained attention as alternatives to conventional nanoscale engines. However, a comprehensive optimization of their performance, which could serve as a benchmark for future engine designs, is still lacking. In this work, we address this gap by deriving and analyzing the optimal driving protocol for a collisional Brownian engine. By maximizing the average output work, we show that the optimal protocol consists of linear force segments separated by impulsive delta-like kicks that instantaneously reverse the particle's velocity. This structure enforces constant velocity within each stroke, enabling fully analytical expressions for optimal output power, efficiency, and entropy production. We demonstrate that the optimal protocol significantly outperforms standard strategies (such as constant, linear, or periodic drivings) achieving higher performance while keeping entropy production under control. Remarkably, when evaluated using realistic experimental parameters, the efficiency approaches near-unity at the power optimum, with entropy production remaining well controlled, a striking feature of the optimal protocol. To analyze a more realistic scenario, we examine the impact of smoothing the delta-like forces by introducing a finite duration and find that, although this reduces efficiency and increases entropy production, the optimal protocol still delivers high power output in a robust manner. Altogether, our results provide a theoretical benchmark for finite-time thermodynamic optimization of Brownian engines under time-periodic drivings.

## I. INTRODUCTION

The study of small-scale engines operating far from equilibrium has gained significant attention in recent years [1–5]. This interest is particularly driven by their relevance in systems where thermal fluctuations are no longer negligible, such as colloidal particles [6–13], biomolecular motors [14–20] and quantum dots [21–25]. In these regimes, classical thermodynamic approaches fall short, and a more refined description is offered by stochastic thermodynamics, which captures the role of fluctuations, dissipation, and energy conversion at the microscopic level. One of the main challenges in this context is to extract useful work in finite time while managing entropy production—an issue that has been addressed through a variety of proposed setups, including, for example, collective systems [26–30] and driving protocols tailored to optimize either efficiency or power [31–39].

Among them, Brownian engines stand out as both theoretically rich and experimentally accessible platforms, capable of shedding light on the fundamental limits of performance under non-equilibrium conditions. These systems, typically realized with colloidal particles in time-dependent potentials [6–8, 13] or optically driven traps [10], provide precise control and measurement of work, heat, and fluctuations, making them ideal candidates for exploring how microscopic dynamics translate into thermodynamic behavior. In such setups, a crucial aspect is the driving protocol—the way in which external forces are applied to the system, shaping its interaction with the environment. One particularly well-studied case is that of engines driven by stiffness modulation, for which optimal protocols have been determined in both passive and, more recently, active scenarios [32, 33, 40–49], setting useful performance benchmarks and deepening our understanding of control at small scales. In parallel, focus has shifted to collisional Brownian engines, where a particle confined in a static potential is driven by external forces that directly alter its momentum. Many studies have explored ways to optimize col-

lisional engines' performance by carefully tuning the driving protocol [30, 35–39, 50–53], shedding light on key aspects of protocol design for these systems. Despite this progress, however, a universally optimal protocol (hereafter OP) that serves as an upper limit for the performance of such systems remains elusive.

In this paper, we aim to address this gap by exploring the OP for collisional Brownian engines, focusing on systems where a single particle interacts sequentially with a thermal reservoir and is subjected to a specific work source at each stage. To determine the OP, we use the ideas of Refs. [32, 33] for the most general case of a collisional Brownian engine described by an underdamped Langevin equation subjected to an external driving force. From this framework, we derive an exact expression for the OP, which includes delta jumps as a key feature, a hallmark also seen in stiffness modulation protocols [32, 33, 40–49, 54]. We then compare the performance of this OP with existing protocols in the literature and analyze how the presence of realistic delta-like functions affects the engine's performance, providing deeper insights into the optimization of work extraction in nonequilibrium Brownian systems. This study establishes the OP as a benchmark for future research, setting a theoretical upper bound on the performance of collisional Brownian engines and paving the way for further advancements in engine optimization.

This paper is organized as follows: In Section II, we present the model, introduce the key analytical expressions for the most general (underdamped) regime, and outline the optimization procedures. Section III is devoted to deriving the OP alongside explicit formulas for key thermodynamic quantities, such as power, efficiency, and entropy production. In Section IV, we benchmark the OP against well-established protocols from the literature. Section V examines the realistic impact of finite-width delta functions on the performance of the optimal Brownian engine. Finally, conclusions and perspectives are summarized in Section VI.

## II. THERMODYNAMIC OVERVIEW OF COLLISIONAL BROWNIAN ENGINES

Consider a Brownian engine where a particle, confined in a harmonic potential, interacts with two thermal reservoirs at temperatures  $T_1$  and  $T_2$ . The engine operates in cycles, during which the particle stays in contact with the reservoir at  $T_1$  for a time  $\tau_1$  and with the one at  $T_2$  for the remaining interval  $\tau - \tau_1$ . While coupled to a bath, the particle exchanges energy as a time-dependent external force is applied, injecting or extracting work from the system. Transitions between reservoirs are idealized as adiabatic processes.

In order to find the OP for this type of engine, we consider the most general case of an underdamped Brownian particle of mass  $m$  trapped in a harmonic potential of (fixed) stiffness  $k$  and driven by a periodic external force  $F_i(t)$ . This system evolves according to

$$m \ddot{x}_i = -\gamma \dot{x}_i + \tilde{F}_i(x, t) + \xi_i(t) \quad (1)$$

where  $\gamma$  represents the viscous coefficient,  $\tilde{F}_i(x, t) = -kx + F_i(t)$  and  $\xi_i(t)$  is the stochastic force following the standard white noise properties  $\langle \xi_i(t) \rangle = 0$  and  $\langle \xi_i(t) \xi_j(t') \rangle = 2\gamma k_B T_i \delta_{ij} \delta(t - t')/m$ . Instead of focusing directly on trajectories, we analyze the evolution of the phase-space probability density  $P_i(x, \dot{x}, t)$ , which follows the Fokker-Planck-Kramers equation

$$\frac{\partial P_i}{\partial t} = - \left[ \dot{x} \frac{\partial P_i}{\partial x} + \tilde{F}_i(x, t) \frac{\partial P_i}{\partial \dot{x}} + \frac{\partial J_i}{\partial \dot{x}} \right], \quad (2)$$

where  $J_i$  is a current of probability given by

$$J_i = -\gamma \dot{x} P_i - \frac{\gamma k_B T_i}{m} \frac{\partial P_i}{\partial \dot{x}}. \quad (3)$$

This framework lead to a Gaussian distribution for  $P_i(x, \dot{x}, t)$  due to the white noise and the linearity of the deterministic forces. In the absence of driving forces ( $F_i(t) = 0$ ) and when the temperatures are equal, the system relaxes to thermal equilibrium, described by the Boltzmann distribution. Deviations from thermal equilibrium arise when the system is subjected to temperature gradients and/or time-dependent external forces, driving it toward a nonequilibrium steady state (NESS). In this regime, the time evolution of the mean energy,  $U_i(t) = m\langle \dot{x}_i^2 \rangle/2 + k\langle x_i^2 \rangle/2$ , can be obtained from Eq. (2) and takes the form of a sum of two contributions, namely  $\dot{U}_i(t) = -[\dot{W}_i(t) + \dot{Q}_i(t)]$ , where

$$\dot{W}_i(t) = -F_i(t) \langle \dot{x}_i \rangle(t) \quad (4)$$

represents the power delivered from/to the particle by the external driving during stroke  $i$  and

$$\dot{Q}_i(t) = \gamma \left( \langle \dot{x}_i^2 \rangle(t) - \frac{k_B T_i}{m} \right). \quad (5)$$

is the heat exchanged with the external bath during the same stroke. The driving force is split into two parts, each corresponding to one stroke of the cycle, namely

$$F_i(t) = \begin{cases} X_1 g_1(t), & 0 \leq t < \tau_1, \\ X_2 g_2(t), & \tau_1 \leq t < \tau, \end{cases} \quad (6)$$

where  $X_i$  is the strength of the thermodynamic force applied in each stage and  $g_i(t)$  defines the protocol shape over the corresponding interval. When averaged over a cycle,  $\overline{U} = \overline{W}_1 + \overline{W}_2 + \overline{Q}_1 + \overline{Q}_2 = 0$ , consistent with the first law of thermodynamics. The second law of thermodynamics is derived by taking the time derivative of the Shannon entropy  $S_i = -k_B \langle \ln P_i \rangle$ , along with Eq. (2), leading to the relation  $\dot{S}_i = \sigma_i(t) - \Phi_i(t)$ , where the entropy production  $\sigma_i(t)$  and the entropy flux  $\Phi_i(t)$  are given by

$$\sigma_i(t) = \frac{m}{\gamma T_i} \int \frac{J_i^2}{P_i} dx d\dot{x} \quad \text{and} \quad \Phi_i(t) = \frac{\dot{Q}_i(t)}{T_i}. \quad (7)$$

Consistent with the second law,  $\sigma_i(t)$  is always non-negative. Using the first law of thermodynamics, the fact that  $\sigma_i(t) = \Phi_i(t)$  in the NESS and defining the temperatures  $T_1$  and  $T_2$  in terms of their average  $T = (T_1 + T_2)/2$  and their difference  $\Delta T = T_2 - T_1$ , we can rewrite the entropy production rate averaged over a complete cycle in the following general form:

$$\bar{\sigma} = \frac{4T^2}{4T^2 - \Delta T^2} \left[ \frac{-(\overline{W}_1 + \overline{W}_2)}{T} + \frac{(\overline{Q}_1 - \overline{Q}_2) \Delta T}{2T^2} \right]. \quad (8)$$

In order to compare our protocol with existing studies, we focus on the simplest scenario of a work-to-work converter, a system where energy input, whether chemical or mechanical, is converted into useful power output. This class of systems has been extensively studied in the literature, both theoretically [3, 55–58] and experimentally [10, 18, 19]. In this case, temperatures are equal ( $\Delta T = 0$ ) and the system is driven by only two thermodynamic forces, directly associated with  $X_1$  and  $X_2$ . Therefore, Eq. (8) simplifies to

$$\bar{\sigma} = \frac{-(\overline{W}_1 + \overline{W}_2)}{T}. \quad (9)$$

In the linear response regime, Eq. (9) can be expressed as the sum of thermodynamic forces  $f_i = X_i/T$  times thermodynamic fluxes  $J_i$ , namely  $\bar{\sigma} = J_1 f_1 + J_2 f_2$ , where

$$\overline{W}_1 = -T J_1 f_1 = -T(L_{11} f_1^2 + L_{12} f_1 f_2), \quad (10)$$

$$\overline{W}_2 = -T J_2 f_2 = -T(L_{22} f_2^2 + L_{21} f_2 f_1), \quad (11)$$

in which  $L_{ij}$ 's represents the Onsager coefficients. Two points are worth highlighting. First, since we are dealing with work-to-work converters, no coupling exists between work fluxes

and heat flux, implying that the Onsager coefficients that involve temperature are all zero. Second, expressions in the form of Eqs. (10) and (11) are obtained when we average Eq. (4) over a complete cycle.

Finally, a work-to-work engine converts a portion of the input power  $\overline{W}_{\text{in}}$  into useful output power  $\overline{W}_{\text{out}}$ , where  $\overline{W}_{\text{in}} < 0$ ,  $\overline{W}_{\text{out}} \geq 0$  and  $|\overline{W}_{\text{in}}| > |\overline{W}_{\text{out}}|$ . We can thus define the efficiency of the converter as

$$\eta \equiv -\frac{\overline{W}_{\text{out}}}{\overline{W}_{\text{in}}}. \quad (12)$$

In terms of the Onsager coefficient, where we use  $i$  for the input and  $j$  for the output force, we have

$$\eta = -\frac{J_j f_j}{J_i f_i} = -\frac{L_{jj} f_j^2 + L_{ji} f_i f_j}{L_{ii} f_i^2 + L_{ij} f_j f_i}. \quad (13)$$

As a last comment, we highlight that, as stated in Ref. [53], the optimized value of both power and efficiency can be obtained solely in terms of the Onsager coefficients. Indeed, for a fixed  $f_i$ , the force  $f_j^{\text{MP}}$  delivering the maximum power is given by  $f_j^{\text{MP}} = -L_{ji} f_i / 2L_{jj}$ , with respective maximum power and efficiency given by

$$\mathcal{P}_{\text{MP}} = T \frac{L_{ji}^2}{4L_{jj}} f_i^2, \quad \eta_{\text{MP}} = \frac{L_{ji}^2}{4L_{jj} L_{ii} - 2L_{ji} L_{ij}}. \quad (14)$$

Similarly, one finds the force that optimizes efficiency, as well as the optimal efficiency itself, to be

$$f_j^{\text{ME}} = \frac{L_{ii}}{L_{ij}} \left( -1 + \sqrt{1 - \frac{L_{ji} L_{ij}}{L_{jj} L_{ii}}} \right) f_i, \quad (15)$$

$$\eta_{\text{ME}} = -\frac{L_{ji}}{L_{ij}} + \frac{2L_{ii} L_{jj}}{L_{ij}^2} \left( 1 - \sqrt{1 - \frac{L_{ij} L_{ji}}{L_{ii} L_{jj}}} \right). \quad (16)$$

### III. OPTIMAL PROTOCOL

With the thermodynamics of Brownian engines established, we now shift our attention to the central result of this work. Inspired by Refs. [32, 33], we seek the protocol  $F(t)$  that maximizes the integral

$$\overline{W} = -\frac{1}{\tau} \int_{\tau_a}^{\tau_b} F(t) \langle \dot{x} \rangle dt, \quad (17)$$

where  $\tau_a = 0$  ( $\tau_1$ ) and  $\tau_b = \tau_1$  ( $\tau$ ) for the output (input) work. By using the Langevin equation (1) for the averaged quanti-

ties, we can express the mean output work rate as

$$\begin{aligned} \overline{W}_{\text{out}} &= -\frac{1}{\tau} \int_0^{\tau_1} [\gamma \langle \dot{x} \rangle + k \langle x \rangle + m \langle \ddot{x} \rangle] \langle \dot{x} \rangle dt \\ &= -\frac{1}{\tau} \left[ \int_0^{\tau_1} \gamma \langle \dot{x} \rangle^2 dt + \frac{k}{2} \langle x \rangle^2 \Big|_0^{\tau_1} + \frac{m}{2} \langle \dot{x} \rangle^2 \Big|_0^{\tau_1} \right]. \end{aligned} \quad (18)$$

To determine the protocol, we apply the Euler-Lagrange equation to minimize the remaining integral in Eq. (18), where the minus sign in the power expression ensures that minimizing the integrand is equivalent to maximizing the power output. This leads to the condition  $\langle \ddot{x} \rangle = 0$ , solved by  $\langle x_i(t) \rangle = v_i t + x_{0i}$ , with  $v_i = \langle \dot{x}_i \rangle = \text{constant}$ . Interestingly, the velocity profile that optimizes the performance of the Brownian engine coincides with the one that minimizes the work in a stiffening trap, as shown in previous works [32, 33]. By applying the boundary conditions  $\langle x_1(0) \rangle = \langle x_2(\tau) \rangle$  and  $\langle x_1(\tau_1) \rangle = \langle x_2(\tau_1) \rangle$ , the number of independent variables is reduced from five,  $\{v_1, v_2, x_{01}, x_{02}, \tau_1\}$ , to three,  $\{v_1, x_{01}, \tau_1\}$ . Two of the remaining variables can be determined by substituting the expressions for  $\langle x_i(t) \rangle$  into the corresponding work equation and maximizing it with respect to  $x_{01}$  and  $\tau_1$ . The maximization of  $\overline{W}_{\text{out}}$  with respect to  $\tau_1$  trivially gives  $\tau_1 = \tau$ , as extending the duration of  $F_{\text{out}}(t)$  increases the extracted work. However, in this limit, only a single stroke remains, and the system no longer operates as a functional engine. For this reason, we instead maximize  $\tau_1$  with respect to the efficiency, yielding  $\tau_1 = \tau/2$ .

At this point, it is important to emphasize that the boundary conditions require the velocity to switch from  $v_1$  to  $v_2 = -v_1$  at  $t = \tau/2$ , and back again at  $t = \tau$ . Since the velocities must remain constant during each stroke, maintaining this condition requires impulsive forces at the transitions, i.e.,

$$F(t) \propto 2m v_1 (\delta(t - \tau) - \delta(t - \tau/2)). \quad (19)$$

Note that the presence of inertia is essential for the cycle to operate properly, as the velocity jumps between strokes require impulsive forces proportional to the system's mass. This implies that the OP can only be realized in systems where inertial effects play a significant role. With all constants determined, the OP is found to be  $F(t) = F_{\text{out}}(t) + F_{\text{in}}(t)$ , where  $F_{\text{out}}$  and  $F_{\text{in}}$  act on  $0 \leq t \leq \tau/2$  and  $\tau/2 \leq t \leq \tau$ , respectively, and are given by

$$F_{\text{out}}(t) = \gamma v_1 + k v_1 \left( t - \frac{\tau}{2} \right) - m v_1 (\delta(t - \tau/2) - \delta(t)), \quad (20)$$

$$F_{\text{in}}(t) = -\gamma v_1 + k v_1 \left( \frac{\tau}{2} - t \right) - m v_1 (\delta(t - \tau/2) - \delta(t - \tau)). \quad (21)$$

The protocol shape, as well as the system dynamics, can be seen in Fig. 1. Notably, the external force acts on the system in such a way that the acceleration is zero, exactly canceling the inertial term. However, at the boundaries, the system can only reset by making jumps in velocity, which highlights the essential role of inertia during stroke transitions. Since the

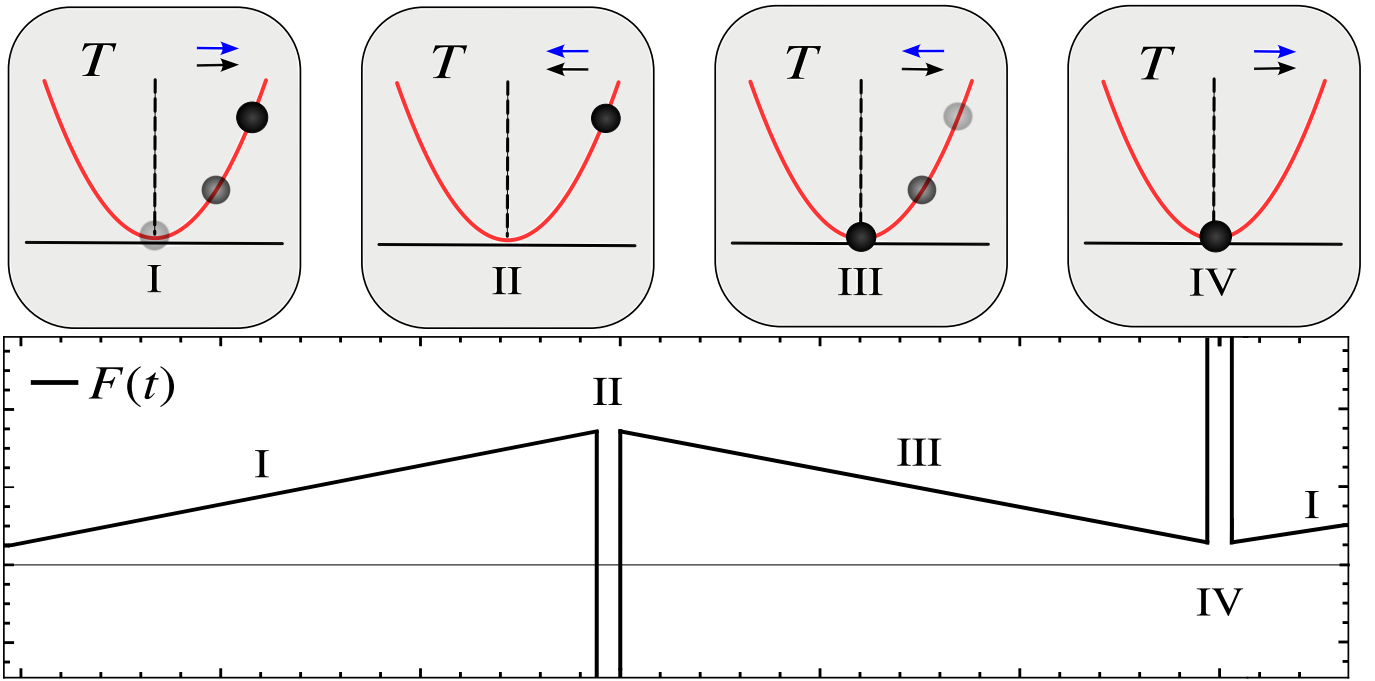


FIG. 1. Schematic representation of the optimal Brownian engine (top) and the corresponding optimal protocol  $F(t)$  (bottom). In the top panel, blue and black arrows indicate the direction of the velocity and the external driving force, respectively. The sharp transitions in steps II and IV correspond to delta-like kicks (amplified for better visualization) that instantaneously reverse the velocity, while steps I and III are the main operational stages. Explicitly, during step I, the protocol increases linearly, exactly compensating the natural acceleration to maintain a constant velocity; in step II, a sudden change reverses the velocity. In step III, the protocol decreases linearly to decelerate the particle while keeping its velocity constant; a final sudden change in step IV reverses the velocity again, preparing the system for the next cycle.

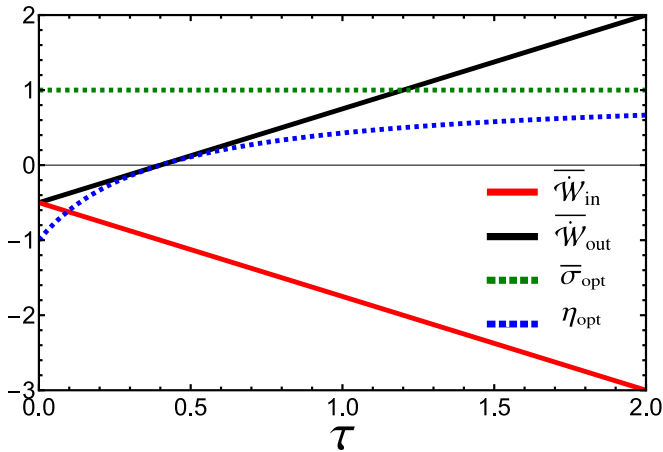


FIG. 2. Input work (red solid line), output work (black solid line), efficiency (blue dashed line), and entropy production (green dashed line) of the optimal protocol as functions of the driving period  $\tau$ . The parameters were set to  $\gamma = 1$ ,  $T = 1$ ,  $v_1 = 1$  and  $k = 10$  to enhance visual clarity.

inertial contributions are sharply localized (delta-like), they can be neglected in the continuous dynamics, eliminating the dependence of the optimal thermodynamic quantities on mass and allowing the protocol to inject energy into the system at no extra energetic cost. These peaks correspond to two preparatory steps (II and IV in Fig. 1) that adjust the system's veloc-

ity before the main strokes (III and I), which contrasts with previous works where only two strokes were required for the system to function as an engine [30, 35–37, 59]. The impact of these preparatory steps on the engine's performance is analyzed in Sec. V.

By substituting  $F(t)$  into Eqs. (17), (12) and (9), we obtain the expressions for the optimal input and output powers, efficiency, and entropy production as

$$\overline{\mathcal{W}}_{\text{in}} = \frac{-v_1^2 (k\tau + 4\gamma)}{8} \quad \text{and} \quad \overline{\mathcal{W}}_{\text{out}} = \frac{v_1^2 (k\tau - 4\gamma)}{8} \quad (22)$$

$$\eta_{\text{opt}} = 1 - \frac{8\gamma}{4\gamma + k\tau} \quad (23)$$

$$\overline{\sigma}_{\text{opt}} = \frac{\gamma}{T} v_1^2 \quad (24)$$

Fig. 2 highlights fundamental characteristics of the system's optimal performance. First, the existence of an external potential is crucial for the system to function as an engine, since the condition  $\eta_{\text{opt}} > 0$  requires  $k\tau > 4\gamma$ . Such a requirement is typically fulfilled in experimental underdamped systems, where  $k\tau \gg \gamma$ . Second, the output work is always smaller than the absolute input work, i.e.,  $\overline{\mathcal{W}}_{\text{out}} < |\overline{\mathcal{W}}_{\text{in}}|$ , meaning that no regime change is observed in the optimal

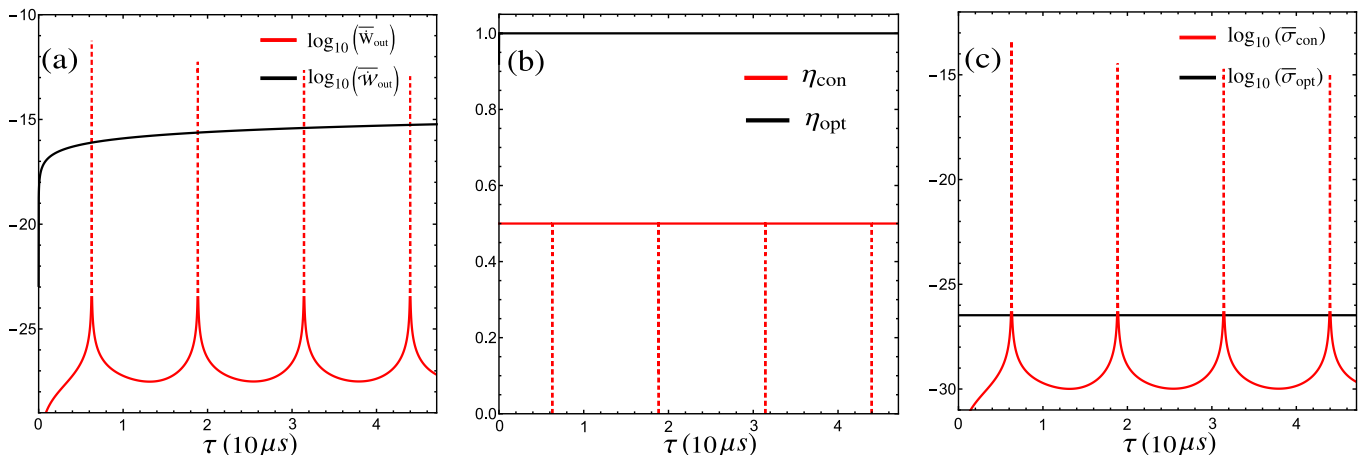


FIG. 3. Panels (a), (b), and (c) show, respectively, the base-10 logarithm of the power, the efficiency, and the base-10 logarithm of the entropy production as functions of the driving period, for both the constant (red lines) and optimal (black lines) protocols. Resonance intervals are indicated by dashed regions. All quantities were computed using the experimental parameters mentioned in the main text. Logarithmic scaling was used in panels (a) and (c) to enhance visualization and allow for a clearer comparison between the protocols.

limit, with the system consistently assigning the first stroke as the useful one and the second as the charging one — a feature that notably differs from previous works where transitions between operational regimes could emerge [59]. Third, since the input and output work scale as  $-\kappa\tau$  and  $+\kappa\tau$ , respectively, this contribution vanishes in the expression for the entropy production, leaving it solely dependent on  $\gamma$ . As a result, power and efficiency can be enhanced by tuning  $k$  and/or  $\tau$  without increasing the entropy production. Fourth, the boundary conditions constrain the dynamics such that only a single thermodynamic force remains (the one proportional to the impulsive force responsible for changing the system’s velocity) which results in the merging of the Onsager coefficients, leading to the expressions in the form  $\bar{\sigma} = (L_{ii} + L_{ij} + L_{ji} + L_{jj})f^2$  for the entropy production and  $\bar{W}_i = (L_{ii} + L_{ij})f^2$  for work, where  $f \propto 2m v_1 \delta(t - t')$  and can be determined analytically once the duration of the preparatory steps is specified.

Finally, since the entropy production in each stroke satisfies  $\bar{\sigma}_i \propto -\bar{W}_i$ , maximizing (minimizing) the average work naturally leads to a minimization (maximization) in entropy production. Indeed, in the output stroke, the optimal force is designed to extract the maximum possible work from the system, which leads to a global minimum in entropy production. In the input stroke, the goal is to restore the system using the least amount of energy, which means making the work input as small (in magnitude) as possible. This results in a local minimum in entropy production, constrained by the imposed boundary condition  $v_2 = -v_1$ . Because of this constraint, the total entropy production is not globally minimized across all possible protocols, but it is minimized within the class of protocols that respect this symmetry. In fact,  $\bar{\sigma}_i$  typically scales with  $|\bar{W}_i|$ , so protocols that produce less work often dissipate less than  $\bar{\sigma}_{\text{opt}}$ . The advantage of the OP is that it can produce much more work at a low dissipation than general protocols.

#### IV. COMPARISON WITH OTHER PROTOCOLS

Several driving protocols for Brownian engines have been examined in the recent literature. Although overdamped dynamics have been more extensively addressed [35–39], it has recently been shown that underdamped systems can exhibit resonant effects that markedly boost performance [59], achieving power and efficiency beyond those attainable in the overdamped regime. Specifically, resonances occur when

$$\tau_{\text{res}} = \frac{2\pi n}{\sqrt{k/m}}, \quad n = 1, 2, 3, \dots \quad (25)$$

Within this context, the most commonly studied drivings are (time) constant, linear, and periodic protocols. Among these, the constant protocol stands out for consistently delivering the best quantitative results, which is why we adopt it as our primary benchmark. Linear and periodic drivings lead to qualitatively similar behaviors and are therefore discussed only briefly. We also include a few remarks on the performance of overdamped systems for comparison. The main analytical expressions for the protocols, as well as for both the underdamped and overdamped regimes, are provided in Appendix A and Appendix B, respectively. To ensure a fair and physically grounded comparison, all performance indicators are evaluated at maximum power, as defined in Eq. (14). For the numerical values, we choose experimentally realistic parameters inspired by previous studies on Brownian engines [6, 10]:  $T = 300 \text{ K}$ ,  $\gamma \approx 10^{-20} \text{ s}^{-1}$ ,  $k \approx \text{pN}/\mu\text{m}$ ,  $m \approx 10^{-18} \text{ kg}$ ,  $\tau \approx 1 \mu\text{s}$  and  $f_i \approx 1 \text{ fN}$ , which correspond to typical velocities around  $v \approx 1 \text{ cm/s}$ .

Insights into the distinct thermodynamic behaviors of the optimal and constant protocols can be drawn from Fig. 3. In panel (a), the OP exhibits a monotonic increase in output power with period, maintaining robust performance around  $10^{-16} \text{ J/s}$ . In contrast, the constant protocol outperforms the OP only within narrow resonance windows (dashed areas),

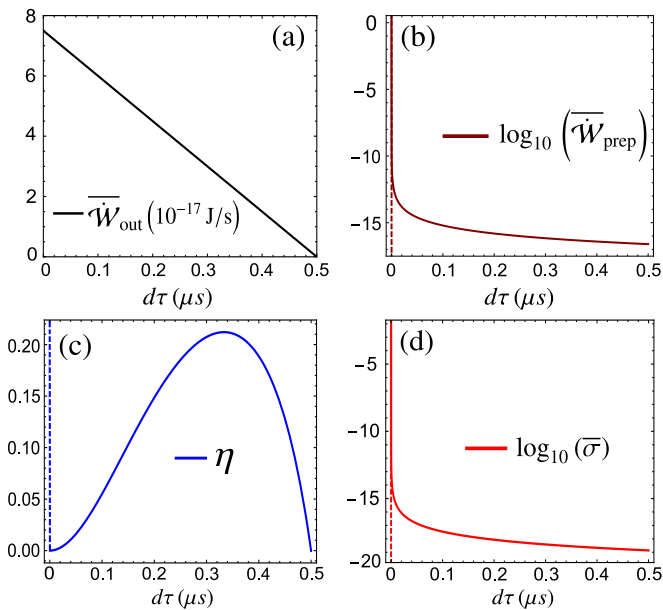


FIG. 4. Performance of the engine as a function of the regularization width  $d\tau$  of the delta contributions. (a) Output power  $\overline{W}_{\text{out}}$ ; (b) Log-10 of the preparation work  $\overline{W}_{\text{prep}}$ ; (c) efficiency  $\eta$ ; (d) Log-10 of the entropy production  $\overline{\sigma}$ . The dashed region in panel (c) indicates the discontinuity in efficiency occurring at  $d\tau = 0$ . We adopt the same parameters as in Fig. 3, fixing the driving period at  $\tau = 6 \mu\text{s}$ .

peaking near  $10^{-11} \text{ J/s}$  and dropping sharply in power outside these regions. Panel (b) shows that the OP sustains near-unity efficiency ( $\eta \approx 0.999\dots$  to the ninth decimal digit) across all periods—a striking result, especially considering that this value is achieved under conditions of global maximum power. The constant protocol, in turn, holds an efficiency near 0.5 for most periods, exhibiting abrupt transitions into non-converting regimes near resonance (which manifest as vertical lines in panel (b)) followed by a return to  $\eta = 0.5$  at exact resonance. In panel (c), the OP maintains a constant entropy production of about  $10^{-26} \text{ J/Ks}$ , roughly ten orders below its power output, reflecting a minimal and controlled dissipation. The constant protocol shows low dissipation most of the time but develops sharp entropy peaks near resonance, reaching up to  $10^{-13} \text{ J/Ks}$ , indicating that its high performance under resonance comes at a significant thermodynamic cost.

For completeness, we briefly compare the performance of other protocols in both damping regimes. In the underdamped regime, the periodic protocol stands out with  $W_{\text{out}} \approx 5.3 \times 10^{-12} \text{ J/s}$  and  $\eta \approx 0.51$ , albeit with an entropy production  $\overline{\sigma} \approx 1.7 \times 10^{-14} \text{ J/Ks}$ , close to that of the constant protocol. The linear protocol performs modestly, with  $W_{\text{out}} \approx 1.75 \times 10^{-23} \text{ J/s}$ ,  $\overline{\sigma} \approx 5.8 \times 10^{-26} \text{ J/Ks}$ , and  $\eta \approx 0.5$ . In the overdamped case ( $\gamma \approx 10^{-8} \text{ s}^{-1}$ ), the constant protocol exhibits the best performance, yielding  $W_{\text{out}} \approx 6 \times 10^{-24} \text{ J/s}$ ,  $\overline{\sigma} \approx 2 \times 10^{-26} \text{ J/Ks}$ , and efficiency  $\eta \approx 0.5$ . The linear and periodic drivings, in contrast, deliver significantly lower performance, with output powers several orders of magnitude below those of the constant protocol.

In summary, although alternative protocols can yield great performance in the underdamped regime, they do so only under narrowly optimized timing conditions, with performance decreasing rapidly outside these settings. overdamped systems, on the other hand, remain far from optimal, exhibiting output powers several orders of magnitude below that of the OP. In contrast, the OP consistently delivers near-maximal efficiency, sustained work extraction, and low entropy production. These features highlight the OP as a robust and thermodynamically advantageous driving strategy.

## V. IMPACT OF DELTA-LIKE FORCES

To better reflect realistic, smooth force exchanges, we replace deltas in  $F(t)$  with narrow Gaussians,  $\delta(t) \rightarrow \mathcal{N}(t, d\tau)$ , with variance  $d\tau$  and centered at the same switching times. Although this substitution makes the mean Langevin equation less tractable analytically, in the experimental regime of interest ( $\gamma \ll k, m \ll k$ ), the approximation  $x(t) \approx F(t)/k$  is accurate. This yields  $v(t) \approx \dot{F}(t)/k$ , and the optimal work per stroke becomes

$$\overline{W}_i \approx -\frac{1}{\tau} \int_{\tau_a}^{\tau_b} F(t) \frac{\dot{F}(t)}{k} dt = -\frac{1}{2k\tau} F(t)^2 \Big|_{\tau_a}^{\tau_b}. \quad (26)$$

The results obtained using this approximation show excellent agreement with numerical results. Here, it is important to notice that the expressions for work have now four contributions, two of them identical to Eq. (22) and two accounting for the preparatory steps (Gaussian contributions). The latter is not considered useful work, but rather an energetic cost required to sustain the cycle, since it occurs over a very short time interval and no extractable work can be obtained from it. This leads to an additional term,  $\overline{W}_{\text{prep}}$ , modifying Eqs. (9) and (12) as

$$\overline{\sigma} = \frac{-\left(\overline{W}_{\text{in}} + \overline{W}_{\text{out}} + \overline{W}_{\text{prep}}\right)}{T} \quad (27)$$

$$\eta = \frac{\overline{W}_{\text{out}}}{\left|\overline{W}_{\text{in}}\right| + \left|\overline{W}_{\text{prep}}\right|} \quad (28)$$

Figure 4 shows how delta-like force contributions influence the engine's performance. The output power (panel (a)) initially matches the value predicted by Eq. (22), then decreases almost linearly as  $d\tau$  increases. Notably, the power vanishes when  $d\tau = \tau/12$ , suggesting a physical lower bound on how long abrupt forces can act (to operate as a converter, the driving must remain sufficiently sharp). For small  $d\tau$ ,  $\overline{W}_{\text{prep}}$  (panel (b)) exceeds the output power by several orders of magnitude, meaning a large energy input is needed just to sustain the cycle. As  $d\tau$  increases, this ratio improves, with  $\overline{W}_{\text{prep}}$  becoming about two orders of magnitude greater than the output—an improvement, but it still reflects a regime where more

energy is spent to maintain the cycle than is extracted from it. This trend also appears in the efficiency  $\eta$ , shown in panel (c). As  $d\tau \rightarrow 0$ , efficiency drops to nearly zero due to the dominance of preparation work. With increasing  $d\tau$ , efficiency rises, peaking at  $\eta = 0.21$  around  $d\tau \approx 0.33 \mu\text{s}$  (corresponding to a power of  $2.6 \times 10^{-17}$  J/s) before declining again. Entropy production  $\bar{\sigma}$  in panel (d) follows a similar trend to  $\overline{\dot{W}}_{\text{prep}}$ , exhibiting high dissipation near  $d\tau = 0$  and decreasing as  $d\tau$  increases, ultimately reaching values up to two orders of magnitude lower than the output power. We finally point out that the dashed regions in panels (a), (b) and (c) indicate discontinuous jumps occurring at exactly  $d\tau = 0$ , where  $\overline{\dot{W}}_{\text{prep}}$  abruptly drops to zero, while entropy production and efficiency shift to their ideal values ( $10^{-26}$  J/Ks and  $\eta \approx 0.999 \dots$ , respectively). This highlights that optimal performance requires extremely sharp (infinitesimal) pulses.

Overall, these results suggest that, although smoothing the delta-like kicks makes the implementation of the OP experimentally feasible, it leads to reduced efficiency and increased entropy production. However, unlike resonant engines that demand extremely fine tuning to achieve peak performance, the OP retains high power output in a robust and controllable manner, even under realistic conditions, manifesting as an effective and reliable choice of driving protocol.

## VI. CONCLUSIONS

In this work, we derived the optimal driving protocol for a collisional Brownian engine driven by external forces. By variationally maximizing the output work, we showed that the OP consists of piecewise-linear force segments that maintain constant velocity by canceling the particle's acceleration, separated by impulsive contributions that instantaneously reverse its direction of motion. This structure globally maximizes the power output while locally minimizing entropy production. Analytical expressions for key thermodynamic quantities, such as output power, efficiency, and entropy production were obtained, allowing for a complete characterization of the engine's performance. The resulting protocol displays exceptional thermodynamic behavior: it achieves both maximum work and near-optimal efficiency, with entropy production remaining several orders of magnitude smaller than the output power. When compared to standard drivings, the OP outperforms them globally in both efficiency and power, while being locally surpassed in power only near resonance. Moreover, its entropy production remains significantly lower than the magnitude of power output, setting it apart from the alternative protocols. To investigate experimental feasibility, we analyzed a more realistic scenario in which the impulsive contributions are smoothed into narrow Gaussian pulses, corresponding to a finite but small time interval  $d\tau$ . Although performance degrades for non-infinitesimal  $d\tau$ , with efficiency decreasing and entropy production increasing compared to the ideal delta case, the protocol still achieves high power robustly and maintains entropy production at manageable levels, demonstrating its viability for practical implementations.

Altogether, our findings establish a new benchmark for finite-time thermodynamic optimization of collisional Brownian engines, highlighting the importance of carefully engineered drivings to optimize the engine performance. They also provide practical insights for designing microscale engines capable of combining high power and low dissipation under realistic physical constraints.

## ACKNOWLEDGMENTS

Authors gratefully acknowledge Yasmin Torres for useful hints in Fig. 1 and Fernando S. Filho for a detailed reading of the manuscript. The financial support from FAPESP under grant number 2022/16192-5 is also acknowledged.

### Appendix A: Main expressions for general underdamped Brownian engines

Building on the framework developed in Ref. [59], the relevant thermodynamic expressions retain the same structure as those derived in Sec. II. A general time-dependent driving can be represented as  $\mathcal{F}(t) = f_i g_i(t)$ , where

$$g_1(t) = \frac{a_0}{2} + \sum a_n \cos\left(\frac{2\pi n t}{\tau}\right) + b_n \sin\left(\frac{2\pi n t}{\tau}\right) \quad \text{and (A1)}$$

$$g_2(t) = \frac{c_0}{2} + \sum c_n \cos\left(\frac{2\pi n t}{\tau}\right) + d_n \sin\left(\frac{2\pi n t}{\tau}\right) \quad \text{(A2)}$$

The driving protocol is defined by selecting the Fourier coefficients  $a_n, b_n, c_n$ , and  $d_n$ , such that  $c_n = d_n = 0$  for the first step ( $i = 1$ ) and  $a_n = b_n = 0$  for the second step ( $i = 2$ ). Notably, the Fourier expansion inherently satisfies the required boundary conditions, i.e., the continuity of the probability distribution at  $t = \tau/2$  and the periodicity condition ensuring that the system returns to its initial state at  $t = \tau$ . Averaging Eq. (1) yields the following general expression for the mean velocity  $\bar{v}(t)$ :

$$\begin{aligned} \bar{v}(t) = \sum_{k=1}^{\infty} (f_1 \cdot a_{1vk} + f_2 \cdot a_{2vk}) \cos\left(\frac{2\pi k t}{\tau}\right) \\ + (f_1 \cdot b_{1vk} + f_2 \cdot b_{2vk}) \sin\left(\frac{2\pi k t}{\tau}\right) \end{aligned} \quad \text{(A3)}$$

where  $a_{ivk}$  and  $b_{ivk}$  denote the Fourier coefficients of the mean velocity, determined by the specific form of the driving forces. By averaging Eq. (4) with  $v(t)$  given by Eq. (A3), one obtains expressions analogous to Eqs. (10) and (11). The general form of the Fourier coefficients of the velocity, along with the corresponding Onsager coefficients, is provided by:

$$a_{1kv} = \frac{8\pi k \tau (8\pi \gamma k \tau a_n + b_n (\tau^2 (\gamma^2 - \omega_D^2) - 16\pi^2 k^2))}{(\tau^2 (\gamma - \omega_D)^2 + 16\pi^2 k^2) (\tau^2 (\gamma + \omega_D)^2 + 16\pi^2 k^2)},$$

$$a_{2kv} = \frac{8\pi k\tau (8\pi\gamma k\tau c_n + d_n (\tau^2 (\gamma^2 - \omega_D^2) - 16\pi^2 k^2))}{(\tau^2 (\gamma - \omega_D)^2 + 16\pi^2 k^2) (\tau^2 (\gamma + \omega_D)^2 + 16\pi^2 k^2)},$$

$$b_{1kv} = \frac{8\pi k\tau (a_n (\tau^2 (\omega_D^2 - \gamma^2) + 16\pi^2 k^2) + 8\pi\gamma k\tau b_n)}{(\tau^2 (\gamma - \omega_D)^2 + 16\pi^2 k^2) (\tau^2 (\gamma + \omega_D)^2 + 16\pi^2 k^2)},$$

$$b_{2kv} = \frac{8\pi k\tau (c_n (\tau^2 (\omega_D^2 - \gamma^2) + 16\pi^2 k^2) + 8\pi\gamma k\tau d_n)}{(\tau^2 (\gamma - \omega_D)^2 + 16\pi^2 k^2) (\tau^2 (\gamma + \omega_D)^2 + 16\pi^2 k^2)},$$

$$L_{11} = T \sum_{n=1}^{\infty} \sum_{k=1}^{\infty} \frac{(\pi k a_{1kv} a_k - b_{1kv} (a_0 ((-1)^k - 1) - \pi k b_k))}{4\pi k} +$$

$$(1 - \delta_{n,k}) \cdot \left( -\frac{((-1)^{k+n} - 1) (k a_n b_{1kv} - n a_{1kv} b_n)}{2\pi (k^2 - n^2)} \right),$$

$$L_{12} = T \sum_{n=1}^{\infty} \sum_{k=1}^{\infty} \frac{(\pi k a_{2kv} a_k - b_{2kv} (a_0 ((-1)^k - 1) - \pi k b_k))}{4\pi k} +$$

$$(1 - \delta_{n,k}) \cdot \left( -\frac{((-1)^{k+n} - 1) (k a_n b_{2kv} - n a_{2kv} b_n)}{2\pi (k^2 - n^2)} \right),$$

$$L_{21} = T \sum_{n=1}^{\infty} \sum_{k=1}^{\infty} \frac{1}{4} \left( a_{1kv} c_k + \frac{c_0 ((-1)^k - 1) b_{1kv}}{\pi k} + b_{1kv} d_k \right) +$$

$$(1 - \delta_{n,k}) \cdot \left( \frac{((-1)^{k+n} - 1) (k b_{1kv} c_n - n a_{1kv} d_n)}{2\pi (k^2 - n^2)} \right),$$

and

$$L_{22} = T \sum_{n=1}^{\infty} \sum_{k=1}^{\infty} \frac{1}{4} \left( a_{2kv} c_k + \frac{c_0 ((-1)^k - 1) b_{2kv}}{\pi k} + b_{2kv} d_k \right) +$$

$$(1 - \delta_{n,k}) \cdot \left( \frac{((-1)^{k+n} - 1) (k b_{2kv} c_n - n a_{2kv} d_n)}{2\pi (k^2 - n^2)} \right),$$

where  $\omega_D = \sqrt{\gamma^2 - 4\kappa}$  is the damped oscillation frequency of the system. The drivings considered include constant, linear, and periodic protocols, which are respectively defined as follows:

$$g_i(t) = \begin{cases} 1, & 0 < t \leq \tau/2, \\ -1, & \tau/2 < t \leq \tau. \end{cases}$$

$$g_i(t) = \begin{cases} \lambda t, & 0 < t \leq \tau/2, \\ \lambda(t - \tau/2), & \tau/2 < t \leq \tau. \end{cases}$$

$$g_i(t) = \begin{cases} \cos\left(\frac{2\pi t}{\tau}\right), & 0 < t \leq \tau/2, \\ \sin\left(\frac{2\pi t}{\tau}\right), & \tau/2 < t \leq \tau. \end{cases}$$

where  $\lambda$  is a constant introduced to ensure that  $g_i(t)$  is dimensionless. The coefficients  $a_n$ ,  $b_n$ ,  $c_n$ , and  $d_n$  are given below. For constant driving:

$$a_0 = c_0 = 1, \quad a_n = c_n = 0, \quad b_n = -d_n = \frac{-1 + (-1)^n}{\pi n}.$$

For linear driving:

$$a_0 = c_0 = \frac{\tau}{4}, \quad a_n = -c_n = \frac{((-1)^n - 1)\tau}{2\pi^2 n^2},$$

$$d_n = -\frac{\tau}{2\pi n}, \quad b_n = (-1)^n d_n.$$

For harmonic driving:

$$a_1 = d_1 = \frac{1}{2}, \quad a_n = d_n = 0 \quad \forall n \neq 1, \quad b_1 = c_1 = 0,$$

$$b_n = \frac{1 + (-1)^n}{(n^2 - 1)\pi} \cdot n = n \cdot c_n \quad \forall n \neq 1, \quad c_0 = -\frac{2}{\pi}.$$

By inserting these coefficients into the expressions for  $a_{1vk}$ ,  $a_{2vk}$ ,  $b_{1vk}$ , and  $b_{2vk}$ , the Onsager coefficients can be directly evaluated.

## Appendix B: Main expressions for general overdamped Brownian Engines

Following Refs. [35–39], here we briefly outline the key features of the overdamped regime. Consider a Brownian particle with mass  $m$  coupled to a thermal bath at temperature  $T_i$ , whose dynamics are governed by the Langevin equation

$$\frac{dv_i}{dt} = -\frac{\alpha}{m} v_i + F_i(t) + \xi_i(t), \quad (\text{B1})$$

This equation can be seen as formally equivalent to that of an overdamped harmonic oscillator subject to a force  $f_i(x) = -\kappa x_i/m$ . This equivalence becomes evident by replacing  $x \rightarrow v$ ,  $\kappa/\alpha \rightarrow \gamma$  and  $1/\alpha \rightarrow \gamma/m$ . Thermodynamic quantities such as work, heat, and entropy production are derived analogously to the underdamped case, using the corresponding Fokker-Planck equation. In this framework, the time evolution of the probability distribution  $P_i(v, t)$  follows

$$\frac{\partial P_i}{\partial t} = -\frac{\partial J_i}{\partial v} - F_i(t) \frac{\partial P_i}{\partial v} \quad (\text{B2})$$

where  $J_i$  represents the probability current given by

$$J_i = -\gamma v P_i - \frac{\gamma k_B T_i}{m} \frac{\partial P_i}{\partial v}, \quad (\text{B3})$$

which matches Eq. (3) in the main text. In the NESS, the mean energy evolves as  $U_i(t) = \frac{1}{2} m \langle v_i^2 \rangle$ , and its time derivative can be decomposed into two contributions identical to those presented in the main text. The same applies to the entropy production. Averaging the instantaneous power  $\dot{W}_i(t)$  over a full cycle yields relations similar to Eqs. (10) and (11), whose Onsager coefficients take the forms found in Refs. [38, 39]:

$$L_{11} = 1 - \frac{2}{\gamma\tau} \tanh\left(\frac{\gamma\tau}{4}\right), \quad (\text{B4})$$

$$L_{12} = \frac{2}{\gamma\tau} \tanh\left(\frac{\gamma\tau}{4}\right), \quad (\text{B5})$$

for constant drivings, where  $L_{11} = L_{22}$  and  $L_{12} = L_{21}$ , and

$$L_{11} = \frac{1}{12\gamma\tau} \left( \gamma^3 \tau^3 - 3(\gamma^2 \tau^2 - 8) \coth\left(\frac{\gamma\tau}{2}\right) - 24 \operatorname{csch}\left(\frac{\gamma\tau}{2}\right) \right), \quad (\text{B6})$$

$$L_{12} = \frac{(-\gamma\tau + 2e^{\frac{\gamma\tau}{2}} - 2) \left( e^{\frac{\gamma\tau}{2}} (\gamma\tau - 2) + 2 \right)}{2\gamma\tau (e^{\gamma\tau} - 1)}, \quad (\text{B7})$$

for linear drivings, where again  $L_{22} = L_{11}$  and  $L_{12} = L_{21}$ .

- 
- [1] K. Sekimoto, [Stochastic Energetics](#), Lecture Notes in Physics (Springer Berlin Heidelberg, 2010).
- [2] C. Jarzynski, [Annual Review of Condensed Matter Physics](#) **2**, 329 (2011).
- [3] U. Seifert, [Reports on Progress in Physics](#) **75**, 126001 (2012).
- [4] C. Van den Broeck and M. Esposito, [Physica A: Statistical Mechanics and its Applications](#) **418**, 6 (2015).
- [5] G. T. Landi and M. Paternostro, [Rev. Mod. Phys.](#) **93**, 035008 (2021).
- [6] I. A. Martínez, É. Roldán, L. Dinis, D. Petrov, J. M. Parrondo, and R. Rica, [Nature physics](#) **12**, 67 (2016).
- [7] J. A. Albay, Z.-Y. Zhou, C.-H. Chang, and Y. Jun, [Scientific reports](#) **11**, 1 (2021).
- [8] S. Rana, P. S. Pal, A. Saha, and A. M. Jayannavar, [Phys. Rev. E](#) **90**, 042146 (2014).
- [9] A. Argun, J. Soni, L. Dabelow, S. Bo, G. Pesce, R. Eichhorn, and G. Volpe, [Phys. Rev. E](#) **96**, 052106 (2017).
- [10] K. Proesmans, Y. Dreher, M. c. v. Gavrilov, J. Bechhoefer, and C. Van den Broeck, [Phys. Rev. X](#) **6**, 041010 (2016).
- [11] I. A. Martínez, É. Roldán, L. Dinis, and R. Rica, [Soft Matter](#) **13**, 22 (2017).
- [12] N. Barros, S. Whitelam, S. Ciliberto, and L. Bellon, [Phys. Rev. E](#) **111**, 044114 (2025).
- [13] V. Blickle and C. Bechinger, [Nature Physics](#) **8**, 143 (2012).
- [14] J. A. C. Albay, Z.-Y. Zhou, C.-H. Chang, H.-Y. Chen, J. S. Lee, C.-H. Chang, and Y. Jun, [Phys. Rev. Res.](#) **5**, 033208 (2023).
- [15] F. Ritort, “Nonequilibrium fluctuations in small systems: From physics to biology,” in [Advances in Chemical Physics](#) (John Wiley and Sons, Ltd, 2007) Chap. 2, pp. 31–123.
- [16] V. Holubec, S. Steffenoni, G. Falasco, and K. Kroy, [Phys. Rev. Res.](#) **2**, 043262 (2020).
- [17] V. Holubec and R. Marathe, [Phys. Rev. E](#) **102**, 060101 (2020).
- [18] S. Liepelt and R. Lipowsky, [Phys. Rev. Lett.](#) **98**, 258102 (2007).
- [19] S. Liepelt and R. Lipowsky, [Phys. Rev. E](#) **79**, 011917 (2009).
- [20] P. De Los Rios and A. Barducci, [eLife](#) **3**, e02218 (2014).
- [21] E. Sübrt and P. Chvosta, [Journal of Statistical Mechanics: Theory and Experiment](#) **2007**, P09019 (2007).
- [22] M. Esposito, R. Kawai, K. Lindenberg, and C. Van den Broeck, [Phys. Rev. E](#) **81**, 041106 (2010).
- [23] F. S. Filho, C. E. Fernández Noa, C. E. Fiore, B. Wijns, and B. Cleuren, [Journal of Physics A: Mathematical and Theoretical](#) **57**, 345001 (2024).
- [24] J. L. D. de Oliveira, M. Rojas, and C. Filgueiras, [Phys. Rev. E](#) **104**, 014149 (2021).
- [25] P. E. Harunari, C. E. Fiore, and K. Proesmans, [Journal of Physics A: Mathematical and Theoretical](#) **53**, 374001 (2020).
- [26] H. Vroylandt, M. Esposito, and G. Verley, [Europhysics Letters](#) **120**, 30009 (2018).
- [27] F. S. Filho, G. A. L. Forão, D. M. Busiello, B. Cleuren, and C. E. Fiore, [Phys. Rev. Res.](#) **5**, 043067 (2023).
- [28] A. Rolandi, P. Abiuso, and M. Perarnau-Llobet, [Phys. Rev. Lett.](#) **131**, 210401 (2023).
- [29] D. Kolisnyk and G. Schaller, [Phys. Rev. Appl.](#) **19**, 034023 (2023).
- [30] I. N. Mamede, P. E. Harunari, B. A. N. Akasaki, K. Proesmans, and C. E. Fiore, [Phys. Rev. E](#) **105**, 024106 (2022).
- [31] F. L. Curzon and B. Ahlborn, [American Journal of Physics](#) **43**, 22 (1975).
- [32] T. Schmiedl and U. Seifert, [Phys. Rev. Lett.](#) **98**, 108301 (2007).
- [33] A. Gomez-Marin, T. Schmiedl, and U. Seifert, [The Journal of Chemical Physics](#) **129**, 024114 (2008).
- [34] N. Golubeva and A. Imparato, [Phys. Rev. Lett.](#) **109**, 190602 (2012).
- [35] F. S. Filho, B. A. N. Akasaki, C. E. F. Noa, B. Cleuren, and C. E. Fiore, [Phys. Rev. E](#) **106**, 044134 (2022).
- [36] I. N. Mamede, A. L. L. Stable, and C. E. Fiore, [Phys. Rev. E](#) **106**, 064125 (2022).
- [37] P. E. Harunari, F. S. Filho, C. E. Fiore, and A. Rosas, [Phys. Rev. Res.](#) **3**, 023194 (2021).
- [38] A. L. L. Stable, C. E. F. Noa, W. G. C. Oropesa, and C. E. Fiore, [Phys. Rev. Res.](#) **2**, 043016 (2020).
- [39] C. E. F. Noa, A. L. L. Stable, W. G. C. Oropesa, A. Rosas, and C. E. Fiore, [Phys. Rev. Res.](#) **3**, 043152 (2021).
- [40] S. Blaber and D. A. Sivak, [Journal of Physics Communications](#) **7**, 033001 (2023).
- [41] R. Garcia-Millan, J. Schüttler, M. E. Cates, and S. A. M. Loos,

- (2024), [arXiv:2407.18542](https://arxiv.org/abs/2407.18542).
- [42] S. A. M. Loos, S. Monter, F. Ginot, and C. Bechinger, *Phys. Rev. X* **14**, 021032 (2024).
- [43] M. V. S. Bonança and S. Deffner, *The Journal of Chemical Physics* **140**, 244119 (2014).
- [44] L. P. Kamizaki, M. V. S. Bonança, and S. R. Muniz, *Phys. Rev. E* **106**, 064123 (2022).
- [45] P. Nazé, S. Deffner, and M. V. S. Bonança, *Journal of Physics Communications* **6**, 083001 (2022).
- [46] M. C. Engel, J. A. Smith, and M. P. Brenner, *Phys. Rev. X* **13**, 041032 (2023).
- [47] A. Zhong and M. R. DeWeese, *Phys. Rev. E* **106**, 044135 (2022).
- [48] S. Whitelam, *Phys. Rev. X* **13**, 021005 (2023).
- [49] E. Aurell, C. Mejía-Monasterio, and P. Muratore-Ginanneschi, *Phys. Rev. E* **85**, 020103 (2012).
- [50] V. Holubec, *Journal of Statistical Mechanics: Theory and Experiment* **2014**, P05022 (2014).
- [51] K. Proesmans and C. Van den Broeck, *Chaos: An Interdisciplinary Journal of Nonlinear Science* **27**, 104601 (2017).
- [52] K. Proesmans and C. Van den Broeck, *Phys. Rev. Lett.* **115**, 090601 (2015).
- [53] K. Proesmans, B. Cleuren, and C. Van den Broeck, *Phys. Rev. Lett.* **116**, 220601 (2016).
- [54] Y. B. Band, O. Kafri, and P. Salamon, *Journal of Applied Physics* **53**, 8 (1982).
- [55] M. F. K. Pebeu, R. L. Woulaché, and T. C. Kofane, *Phys. Rev. E* **98**, 052107 (2018).
- [56] M. E. Fisher and A. B. Kolomeisky, *Proceedings of the National Academy of Sciences of the United States of America* **96**, 6597 (1999).
- [57] D. M. Busiello and C. E. Fiore, *Journal of Physics A: Mathematical and Theoretical* **55**, 485004 (2022).
- [58] H. Hooyberghs, B. Cleuren, A. Salazar, J. O. Indekeu, and C. Van den Broeck, *The Journal of Chemical Physics* **139**, 134111 (2013).
- [59] G. A. L. Forão, F. S. Filho, B. A. N. Akasaki, and C. E. Fiore, *Phys. Rev. E* **110**, 054125 (2024).